Desalination and Water Treatment
www.deswater.com

doi: 10.5004/dwt.2021.27712

237 (2021) 108–120
October

Ultrasound irritation enhanced activation of peroxymonosulfate with Fe^0 for humic acid removal: less formation of Fe-HA complex

Xizhong Bao[a], Yang Zhang[b], Min Zhang[c], Guijue Luo[d], Yue Deng[d], Yong He[e], Yi Zhang[f,*]

[a]*Huber Provincial Academy of Eco-Environmental Sciences, Wuhan, 430070, China, email: 412302347@qq.com*
[b]*Hubei Haomiao Environmental Technology Co., Ltd., Shiyan 442000, China, email: yanghang95101@163.com*
[c]*Cangzhou Xuyang Chemical Co., Ltd., Cangzhou 061113, China, email: a18041156682@163.com*
[d]*China Petroleum & Chemical Corporation Jianghan Oilfield Branch No. 1 Gas Production Plant, Chongqing 400000, China, emails: luoguijue85@dingtalk.com (G. Luo), 15542842413@163.com (G. Luo)*
[e]*Sinopec Jianghan Chongqing Oilfield Branch, Chongqing 400000, China, email: 809877962@qq.com*
[f]*State Key Laboratory of Freshwater Ecology and Biotechnology, Institute of Hydrobiology, Chinese Academy of Sciences, Wuhan 430072, PR China, email: zhangyi@ihb.ac.cn*

Received 24 May 2021; Accepted 12 August 2021

ABSTRACT

Commercial zero-valent iron (Fe^0) particle was used as peroxymonosulfate (PMS) activator with the assistance of ultrasound (US) irritation for humic acid (HA) removal in this study. 100% HA removal rate was obtained in the Fe^0/PMS/US system under the optimal experimental condition. The higher Fe^0 dosage, neutral pH and optimal PMS concentration facilitated the HA removal. The use of US reduced the generation of HA-Fe complex and improved the release of Fe in the Fe^0/PMS/US for HA removal. The reaction process of HA removal was fitted with the first-order kinetic and the US exhibited obvious synergic effect for HA removal. The non-thermal effect of US was the main reason for enhancing HA removal. Sulfate radicals ($SO_4^{\bullet-}$), hydroxyl radicals ($^\bullet OH$), Fe(VI) and singlet oxygen ($^1O_2$) were produced in the reaction and $^1O_2$ was the dominant species according to the result of scavenging tests and electron paramagnetic resonance tests. This study indicates the Fe^0/PMS/US is an available and effective technology for HA removal.

Keywords: Fe^0 particle; Peroxymonosulfate activation; Ultrasound irritation; Humic acid

1. Introduction

The advanced oxidation processes (AOP) are a promising method that has been widely used to treat various organic pollutants with the advantage of low cost, no second pollution and easy operation [1–4]. The main AOP technologies include sulfate activation (including peroxymonosulfate (PMS) activation and persulfate activation), Fenton oxidation, photocatalysis oxidation and ozone oxidation [5–7]. Among these AOP, PMS activation has been paid considerable attention due to the generation of sulfate radical ($SO_4^{\bullet-}$) with high redox potential (2.5–3.1 V) [8–11]. The common methods for PMS activation include metal ion activation, heat activation, UV activation and ultrasound (US) activation [12–15].

Transition metals, such as Fe^{2+}, Mn^{2+} and Ni^{2+}, were widely employed as potential electron donators to activate PMS [16–18]. However, homogeneous PMS activation was limited by the high metal ion and the harsh pH condition in the solution [19,20]. In addition, excessive metal ions in the solution could result in the scavenging of $SO_4^{\bullet-}$. Therefore, the heterogeneous PMS activation, especially iron-based

* Corresponding author.

activator, has been developed for the degradation of varying pollutants [21–23]. Zero-valent iron (Fe^0) is an excellent iron-based material that has been employed in the versatile catalysis fields [24,25]. Fe^0 as PMS activator for pollutant degradation also be focused due to the property of lasting release of iron ion [26–28].

However, the use of Fe^0 for PMS activator is confined by a specific target. The presence of humic acid in the water matrix is usually prone to combine released iron ions to produce the Fe-HA complex on the surface of Fe^0, which impedes the lasting release of iron ions for PMS activation [29,30]. Therefore, the study on the removal of humic acid (HA) in the water matrix has significant importance. To prevent the generation of the Fe-HA complex and the removal of HA, the assistant technology could be developed. In this study, US irradiation was employed as the supporting technology.

Based on the above discussion, the aim of the present study was to: (1) analyze the effect of Fe^0 dosage, pH and PMS concentration on HA removal; (2) investigate the syndetic effect of US on HA removal; (3) compare the change of Fe^0 before and after reaction; (4) explore the possible radical and non-radical for HA removal.

2. Materials and methods

2.1. Materials and instruments

Details of materials and instruments in this study were provided in the supplementary material.

2.2. Experimental work

Details of experimental work in this study were provided in the supplementary material.

2.3. Quenching tests for reactive oxygen species

Details of quenching tests for reactive oxygen species in this study were provided in the supplementary material.

2.4. Thermal effect and non-thermal effect for HA

Details of thermal effect and non-thermal effect for HA in this study were provided in the supplementary material.

2.5. Characterization

Morphology analysis of Fe^0 using scanning electron microscopy and transmission electron microscopy is shown in Fig. 1. Fe^0 particles are irregular shape particles with a size range of 1–60 μm. In addition, the surface of the Fe^0 particle is tight without obvious pores. Based on the Brunauer–Deming–Deming–Teller classification, the N_2 adsorption/desorption isotherm for the Fe^0 (Fig. 2) was closed to the type II with H3 hysteresis loop, which was similar to the nonporous structure. The specific surface area and pore volume of Fe^0 were 0.9 m^2/g and 0.0014 cm^3/g, respectively. In addition, the Brunauer–Emmett–Teller parameter of used Fe^0 (Table 1) had no obvious change, which indicated the sustainable use of Fe^0. Zeta potentials of Fe^0 were measured from pH = 2–12 (Fig. 3) and the pH_{pzc} of Fe^0 was obtained at 3.98.

3. Results and discussion

3.1. HA removal under different reaction systems

Fig. 4 compares the HA removal under different PMS activation systems. The removal rate of HA follow this order: Fe^0/PMS/US (61%) > Fe^0/PMS (43%) > PMS/US (19%) > PMS (15%) > Fe^0/US (nearly 0%) ≈ US (nearly 0%) ≈ Fe^0 (nearly 0%). The use of the only Fe^0, only US and Fe^0/US had almost no effect on HA removal. After 90 min reaction, 43% HA removal was achieved under Fe^0/PMS while 61% under Fe^0/PMS/US. The result indicates the availability of Fe^0/PMS for HA removal and the involvement of US obviously enhanced HA removal.

3.2. Effect of Fe^0 dosage

The effect of Fe^0 dosage on HA removal is shown in Fig. 5. The removal rate of HA significantly increased with the Fe^0 dosage increased from 0.1 to 0.4 g/L. Most of the removal of HA occurred in the first 10 min. The increasing Fe^0 dosage could result in more Fe ion release in solution, which further activated PMS to produce reactive oxygen species (ROS). The pathway of the generation of ROS is shown in Eqs. (1)–(5) [31]. However, the excessive dosage of Fe^0 maybe quenches the generated radical due to the side reaction of released iron ions [32]. In the condition with US, the removal rate of HA was more than without US. In the Fe^0/PMS/US system, a 100% removal rate of HA was obtained at 0.4 g/L Fe^0 dosage. This was due to the HA could be complex with iron ions, which impedes the release of iron ions into solution. The adsorption of HA on Fe^0 was also studied and the HA removal rate was less than 2% in all conditions (Fe^0 dosage from 0.1 to 0.4 g/L, with and without US), which indicated the adsorption was not the main reason for HA removal. In addition, the US played an important role in ROS generation by the synergistic effect of US and Fe^0. The iron concentration in leachate during the reaction was analyzed using ICP-OES (Fig. 6). The first 10 min was the main release process of iron ions. In the condition without US, the release of iron ion was nearly stagnant after the first 10 min while the iron ion was slowly released in the condition of with US. The possible reason was also the formation of the Fe-HA complex on the surface of Fe^0, which impeded the lasting release of iron ions. The use of US could reduce the formation of the Fe-HA complex. This speculation was testified in the characterization section of fresh and used using X-ray photoelectron spectroscopy (XPS).

$$Fe^0 + O_2 + 2H^+ \rightarrow Fe^{2+} + H_2O_2 \quad (1)$$

$$Fe^0 + H_2O_2 \rightarrow Fe^{2+} + 2OH^- \quad (2)$$

$$Fe^0 + 2Fe^{3+} \rightarrow 3Fe^{2+} \quad (3)$$

$$Fe^{2+} + 2HSO_5^- \rightarrow Fe^{3+} + 2^{\bullet}OH + SO_4^{2-} + SO_4^{\bullet-} \quad (4)$$

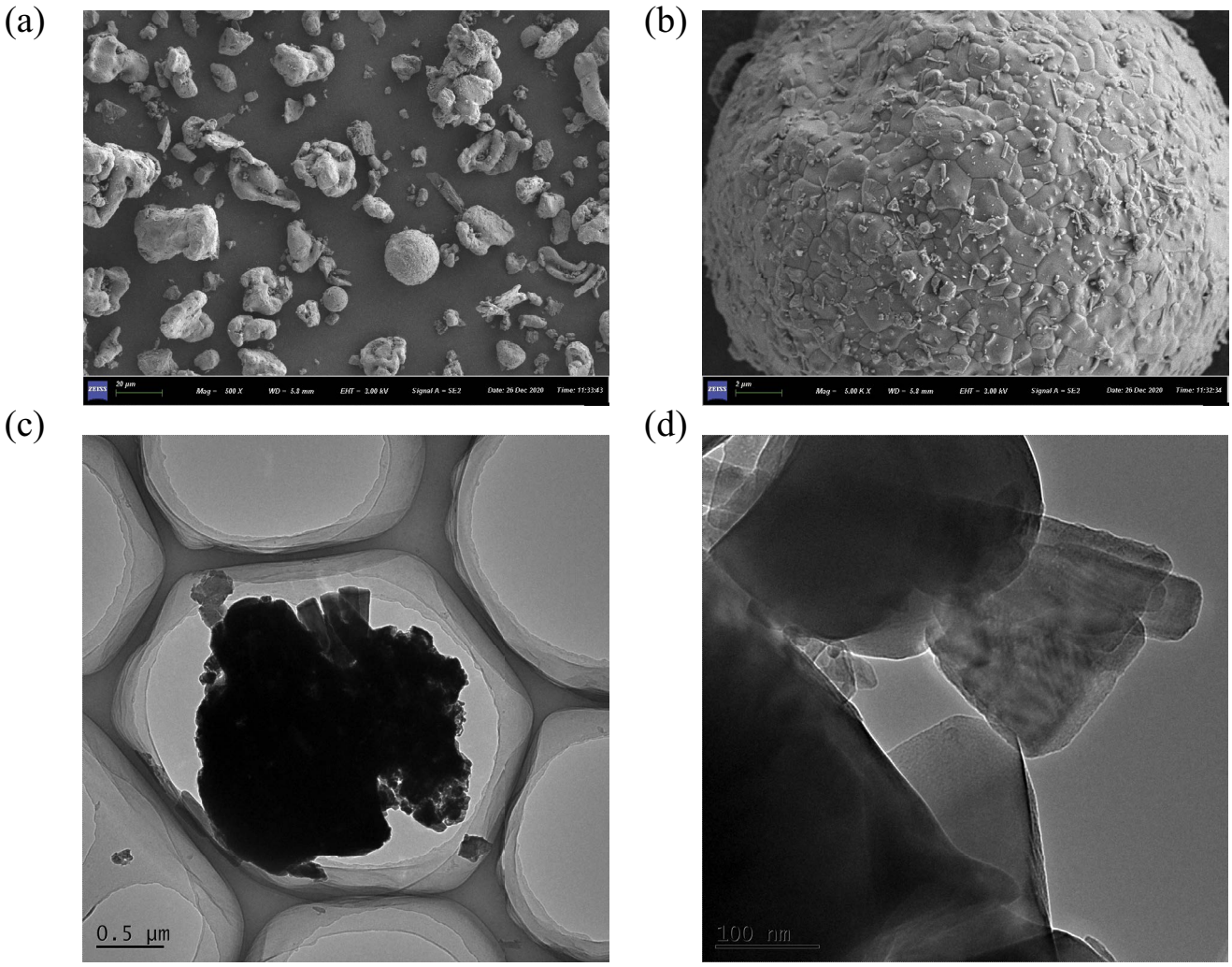

Fig. 1. (a, b) Scanning electron microscopy image of Fe^0 and (c, d) transmission electron microscopy image of Fe^0.

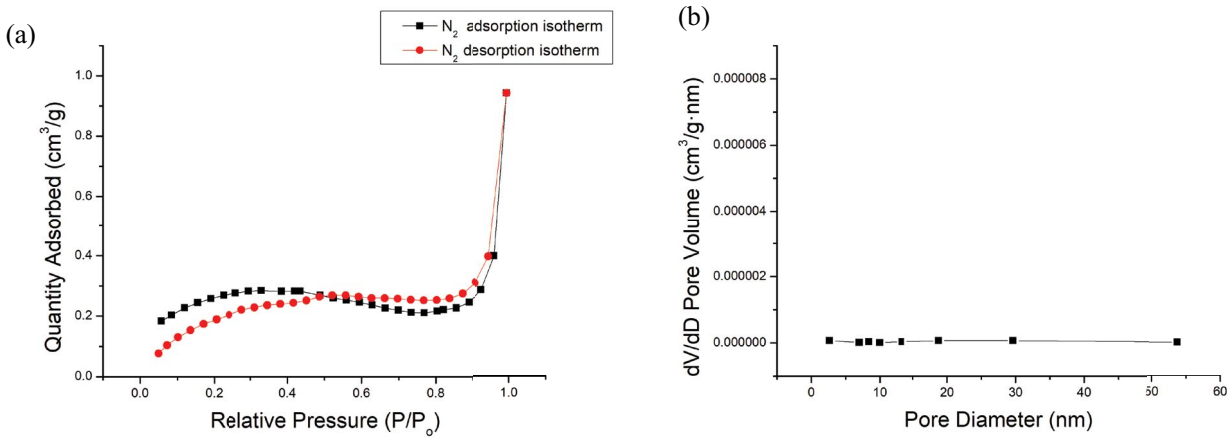

Fig. 2. (a) Nitrogen adsorption–desorption isotherm and (b) pore distribution of Fe^0.

$$H_2O + SO_4^{\bullet -} \rightarrow {}^{\bullet}OH + SO_4^{2-} + H^+ \quad (5)$$

3.3. Effect of PMS concentration

The effect of PMS concentration on HA removal was been studied as depicted in Fig. 7. For both conditions with and without US, optimal PMS concentration for HA removal was 1 mmol/L and the increased PMS concentration was not conductive to the HA removal. The possible reason for this phenomenon was due to the entrapment of free radicals by excessive PMS [Eq. (6)] [33].

$$HSO_5^- + SO_4^{\bullet -} \rightarrow SO_5^{\bullet -} + SO_4^{2-} + H^+ \quad (6)$$

3.4. Effect of initial pH

The effect of initial pH on HA removal is shown in Fig. 8. The optimal initial pH for HA removal was 1 mmol/L. The strong acid and alkaline solution was not conductive to the HA removal. In the acid solution, the iron ion was easily released from the surface of Fe^0, which facilitated the formation of the Fe-HA complex on the surface of Fe^0, resulting in poor HA removal. Compared with the condition of without US, the removal rate was obviously higher with US, which was ascribed to the less formation of Fe-HA complex. In the alkaline solution, for both conditions with and without US, HA was hardly removed. The possible reason was due that (i) the released iron ion was consumed due to the formation of iron hydroxide and (ii) the electrostatic repulsion of Fe^0 and PMS in the solution according to the pH_{pzc} value (3.98) of Fe^0. The change of pH after the reaction was tested (Table S1). The acidity/alkalinity in the acidic/alkaline

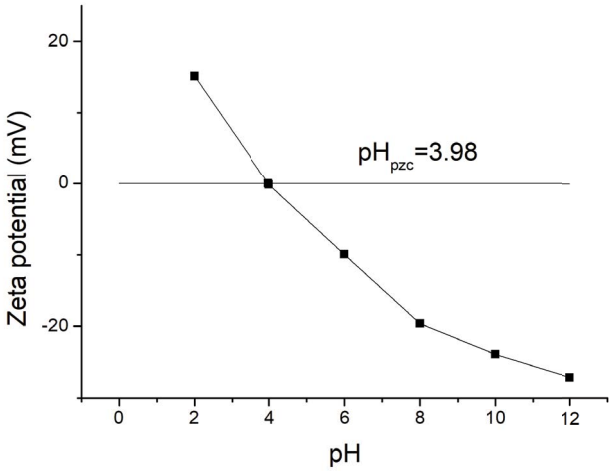

Fig. 3. Zeta potential analysis for Fe^0.

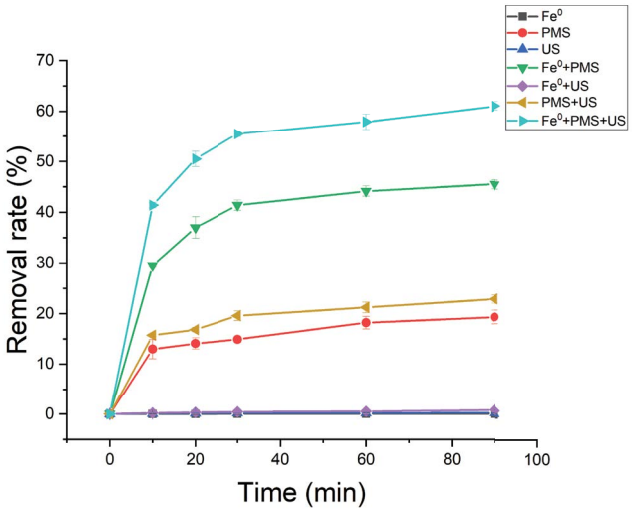

Fig. 4. The removal rate of HA under different reaction system. Experimental parameters: Fe^0: 0.1 g/L dosage; PMS: 1 mmol/L; US 100 W; HA: 10 mg/L; pH: 7.

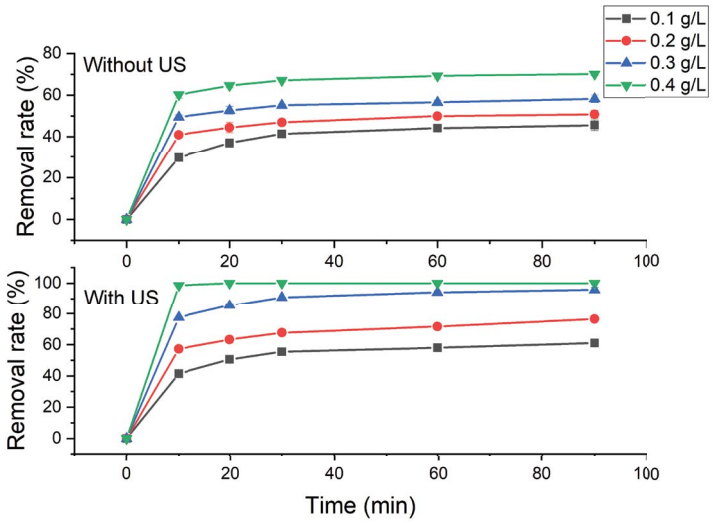

Fig. 5. Effect of different dosages of Fe^0 on HA removal without and with US. Experimental parameters: Fe^0: 0.1–0.4 g/L dosage; PMS: 1 mmol/L; US 100 W; HA: 10 mg/L; pH: 7.

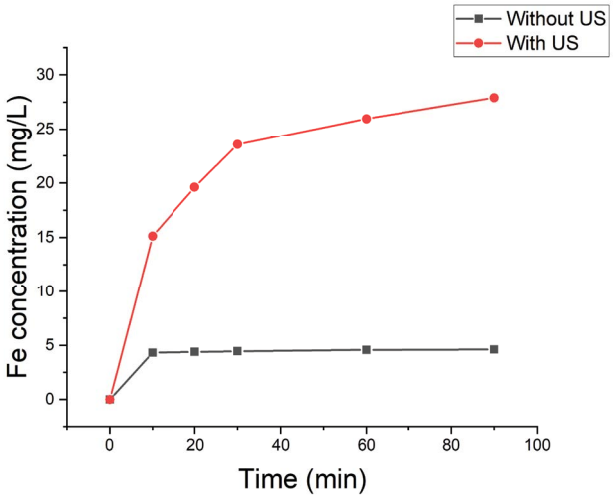

Fig. 6. Fe ion concentration in solution during reaction. Experimental parameters: Fe^0: 0.4 g/L dosage; PMS: 1 mmol/L; US 100 W; HA: 10 mg/L; pH: 7.

solution was slightly reduced, which was imputed to the consumption of H^+/OH^- by released iron ion in solution.

3.5. Kinetic, synergistic effect of US and thermal effects of US for HA removal

Pseudo-first-order kinetic model was used to fit the kinetics of HA removal [Eq. (7)]. According to the obtained k at different systems, the synergy index of US for HA removal under Fe^0/PMS system was determined as Eq. (8):

$$\ln\left(\frac{C_t}{C_0}\right) = -kt \tag{7}$$

$$\text{Synergy Index} = \frac{k_{\text{US/Fe}^0\text{/pms}}}{k_{\text{US/pms}} + k_{\text{Fe}^0\text{/pms}}} \tag{8}$$

where C_0 is initial HA concentrations; C_t is HA concentration measured at time t and k is the reaction rate constant (min^{-1}).

Fig. 9 shows the removal kinetics of HA under a different reaction system. The kinetic fitting was divided into two steps. The kinetic constant k (shown in Table 2) follow this order: Fe^0/PMS/US > Fe^0/PMS > PMS/US > PMS > Fe^0/US ≈ US ≈ Fe^0. In the first 10 min (A section), the kinetic constant k was higher than that in the B section, which indicated the main reaction occurred in the first 10 min. The synergy index of US for HA removal was calculated as 2.03, which indicated synergetic effect from US for HA removal. Fig. 10 shows the thermal effect and non-thermal effect of US on HA removal. In the condition without US, the increased temperature resulted in more HA removal due to the heat activation of PMS. In the condition with US, the increased temperature had no obvious effect on the HA removal, which indicated the non-thermal effect of US resulting in the main HA removal.

3.6. Fe^0 recycling utilization and characterization for HA solution

The recycling utilization of Fe^0 for HA removal was tested and the result was shown in Fig. S1. The Fe^0 particle was separated using a magnet (Fig. S2) and for the fourth cycle experiment. In the condition without US, the HA removal decreased after each recycling utilization. However, in the condition with US, the HA removal decreased relatively slow after each recycling utilization. This was due to the weight loss of Fe^0 particles and the generation of the Fe-HA complex during the reaction. UV-Vis and excitation–emission matrix (Figs. S3 and S4) were used to analyze the HA solution. According to the peak intensity change and change in the characteristic region, the HA content was reduced in the solution. The mineralization degree of HA after reaction and recycling experiment was testified according to total organic carbon (TOC) removal rate (Table S2) [34]. TOC removal rate decreased with recycling time, and the decreasing trend was more obvious without US. The result of the TOC removal rate was consistent with the HA removal rate in each recycling

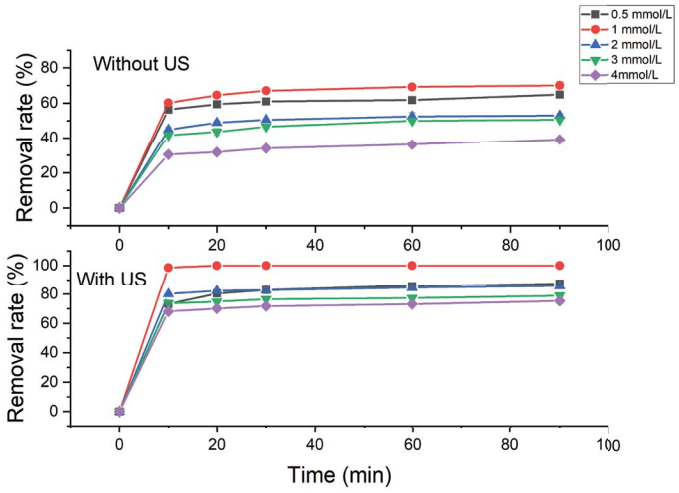

Fig. 7. Effect of different concentrations of PMS on HA removal without and with US. Experimental parameters: Fe^0: 0.4 g/L dosage; PMS: 0.5–4 mmol/L; US 100 W; HA: 10 mg/L; pH: 7.

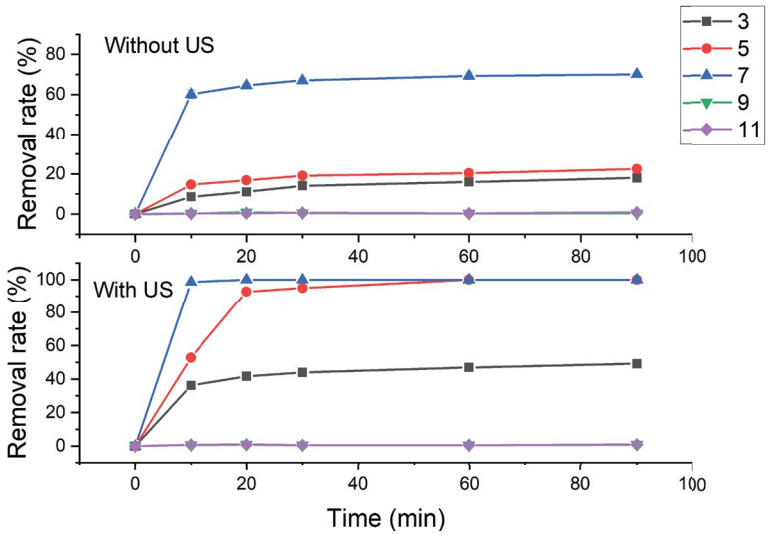

Fig. 8. Effect of different pH on HA removal without US with US. Experimental parameters: Fe^0: 0.4 g/L dosage; PMS: 1 mmol/L; US 100 W; HA: 10 mg/L; pH: 3–11.

Table 1
Brunauer–Emmett–Teller parameters for fresh Fe^0 and used Fe^0

Sample	Specific area (m^2/g)	Volume (cm^3/g)	Average pore diameter (nm)	Average particle diameter (nm)
Fe^0	0.90	0.0014	6.43	6,613
Used Fe^0	0.78	0.0033	6.01	6,479
Used Fe^0 with US	0.97	0.0009	7.52	6,938

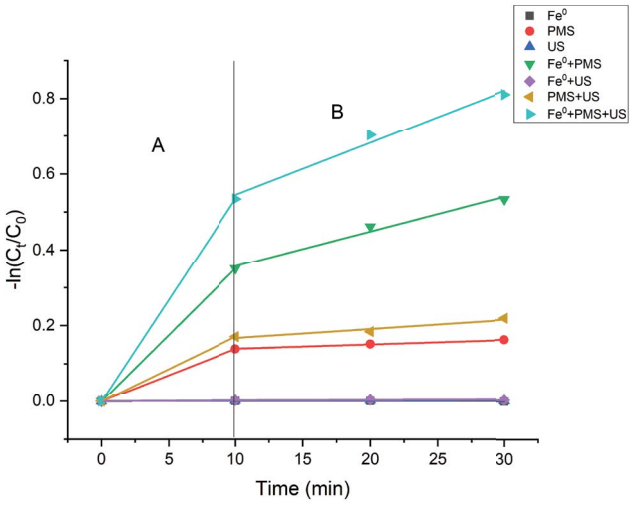

Fig. 9. Removal kinetics of HA under different reaction system. Experimental parameters: Fe^0: 0.1 g/L dosage; PMS: 1 mmol/L; US 100 W; HA: 10 mg/L; pH: 7.

utilization. In addition, the TOC removal rate was relatively low, which indicated HA was not fully mineralized.

The fresh and used Fe^0 particles were characterized using XPS and X-ray diffraction (XRD) to observe the change on the surface of the Fe^0 particle. The XRD pattern of fresh and used Fe^0 particle (Fig. 11) had no obvious change, which was due to the generated oxide and hydroxide on the surface of the Fe^0 particle was too little to be detected. Chemical characteristics of Fe^0 particles were tested by XPS (Fig. 12). In the XPS spectra of Fe 2p, the representative peaks that appeared at 706.6, 710.3 and 712.2 eV were corresponding to Fe^0, Fe(II) and Fe(III), respectively [35,36]. The representative peaks of Fe(II) and Fe(III) were due to the existence of iron hydroxides and oxides on the surface of Fe^0 particles. For fresh and used Fe^0 particles with US, the three representative peaks were all detected, which indicated the surface of Fe^0 particles was not completely covered by oxide. For used Fe^0 particles without US, only the representative peaks of Fe(II) and Fe(III) were detected, which indicated the surface of Fe^0 particles was completely covered by oxide. The result of XPS spectra of Fe 2p demonstrated the use of US in reaction could decrease the generation of iron hydroxides and oxides on the surface of Fe^0 particles. In the XPS spectra of O 1s, the representative peaks that appeared at 530.0, 531.7 and 532.6 eV were corresponding to lattice oxygen (O^{2-}), adsorbed oxygen and C=O group, respectively [37,38]. The lattice oxygen was assigned to the formation of iron (hydr) oxides. The existence of adsorbed oxygen type was due to the water adsorbed on the Fe^0 particle. The appearance of the C=O group was possibly derived from the Fe-HA complex. For used Fe^0 particles without US the three representative peaks were all detected, which indicated the presence of Fe-HA complex. For fresh and used Fe^0 particles with US, only the representative peaks of lattice oxygen (O^{2-}) and

Table 2
The kinetic parameter under different reaction system

	Only Fe^0	Only PMS	Only US	Fe^0 + PMS	Fe^0 + US	Fe^0 + PMS + US
k_A (min^{-1})	2.512E-5	0.0138	1.21E-4	0.01711	2.142E-4	0.0349
k_B (min^{-1})	8.502E-6	0.00112	3.089E-5	0.00235	1.048E-4	0.00922

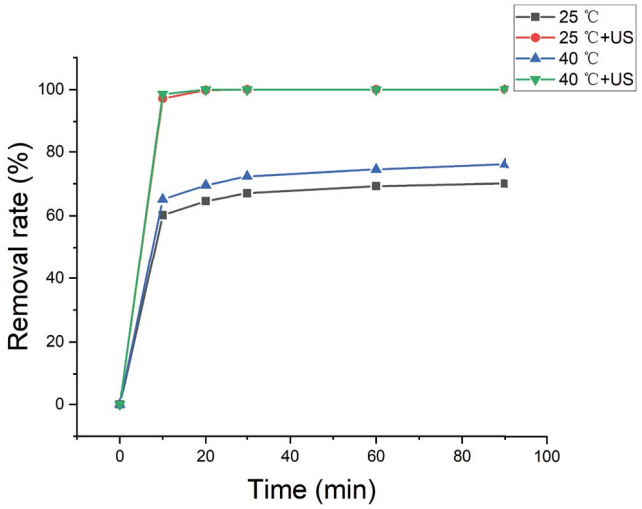

Fig. 10. Effect of thermal effect and non-thermal effect on HA removal. Experimental parameters: Fe^0: 0.4 g/L dosage; PMS: 1 mmol/L; US 100 W; HA: 10 mg/L; pH: 7.

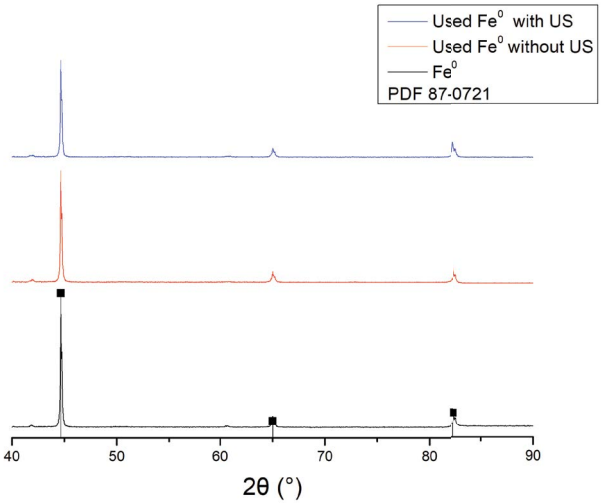

Fig. 11. XRD pattern of Fe^0.

adsorbed oxygen were detected. The result of XPS spectra of O 1s demonstrated the use of US in reaction could decrease the generation of Fe-HA complex on the surface of Fe^0 particle.

3.7. Radical quenching test and electron paramagnetic resonance test

The quenching tests were conducted to test the effect of ROS on HA removal. As literature reported, $OH^•$, $SO_4^{•-}$, $^1O_2$ and Fe(IV) were the possible ROS which involves in the HA removal [35,39–41]. Ethanol was employed as the quenchers for $OH^•$ and $SO_4^{•-}$ due to the high reactivity with both of these species. Tert-butanol was selected as the quenchers for $OH^•$ due to the higher reactivity with $OH^•$ than $SO_4^{•-}$. Dimethyl sulfoxide and tryptophan were employed as the special quenchers for $^1O_2$ and Fe(IV), respectively. The result of radical quenching tests (shown in Fig. 13) indicated that $OH^•$, $SO_4^{•-}$, $^1O_2$ and Fe(IV), all had an effect on the HA removal in the condition without and with US. The order of ROS contribution for HA removal was as following: $^1O_2$ > Fe(IV) > $SO_4^{•-}$ > $OH^•$. An electron paramagnetic resonance (ESR) experiment was carried out to further determine the produced ROS during the reaction. Dimethylpyridine N-oxide (DMPO) was employed as a radical scavenger for $OH^•$ and $SO_4^{•-}$ and 2,2,6,6-tetramethylpiperidine-1-oxyl (TEMPO) was employed to scavenge $^1O_2$. In the condition without US, the signal of DMPO-adduct for $OH^•$ and $SO_4^{•-}$ was not obvious while it became clear with the use of US. The signals of DMPO-$OH^•$, DMPO-$SO_4^{•-}$ and DMPOX were detected with US, which indicated the presence of $OH^•$ and $SO_4^{•-}$ in the reaction, especially with the use of US. However, the signal of TEMPO-$^1O_2$ was obvious in both condition with and without the use of US. The signal intensity of TEMPO-$^1O_2$ was larger with the use of US, which indicated the presence of $^1O_2$ in the reaction. The possible pathway for the generation of $^1O_2$ is as follows [42,43]:

$$Fe^{3+} + H_2O_2 \rightarrow Fe^{2+} + HO_2^• + H^+ \quad (9)$$

$$HO_2^• \rightarrow O_2^{•-} + H^+ \quad (10)$$

$$HO_2^• + O_2^{•-} \rightarrow {}^1O_2 \quad (11)$$

$$2O_2^{•-} + 2H^+ \rightarrow {}^1O_2 + H_2O_2 \quad (12)$$

4. Conclusion

The removal of HA by commercial Fe^0/PMS process with the assistance of US was studied. 100% removal of HA was achieved within 10 min at the optimal reaction conditions: 0.4 g/L Fe^0 dosage, 1 mmol/L PMS, pH at 7 with the assistance of US. The non-thermal effect and synergic effect from US for HA removal were significant. The use of US enhanced the reuse efficiency of Fe^0. The result of XPS indicated the reduced formation of Fe-HA complex and the iron (hydr) oxides with the use of US in the reaction. According to the

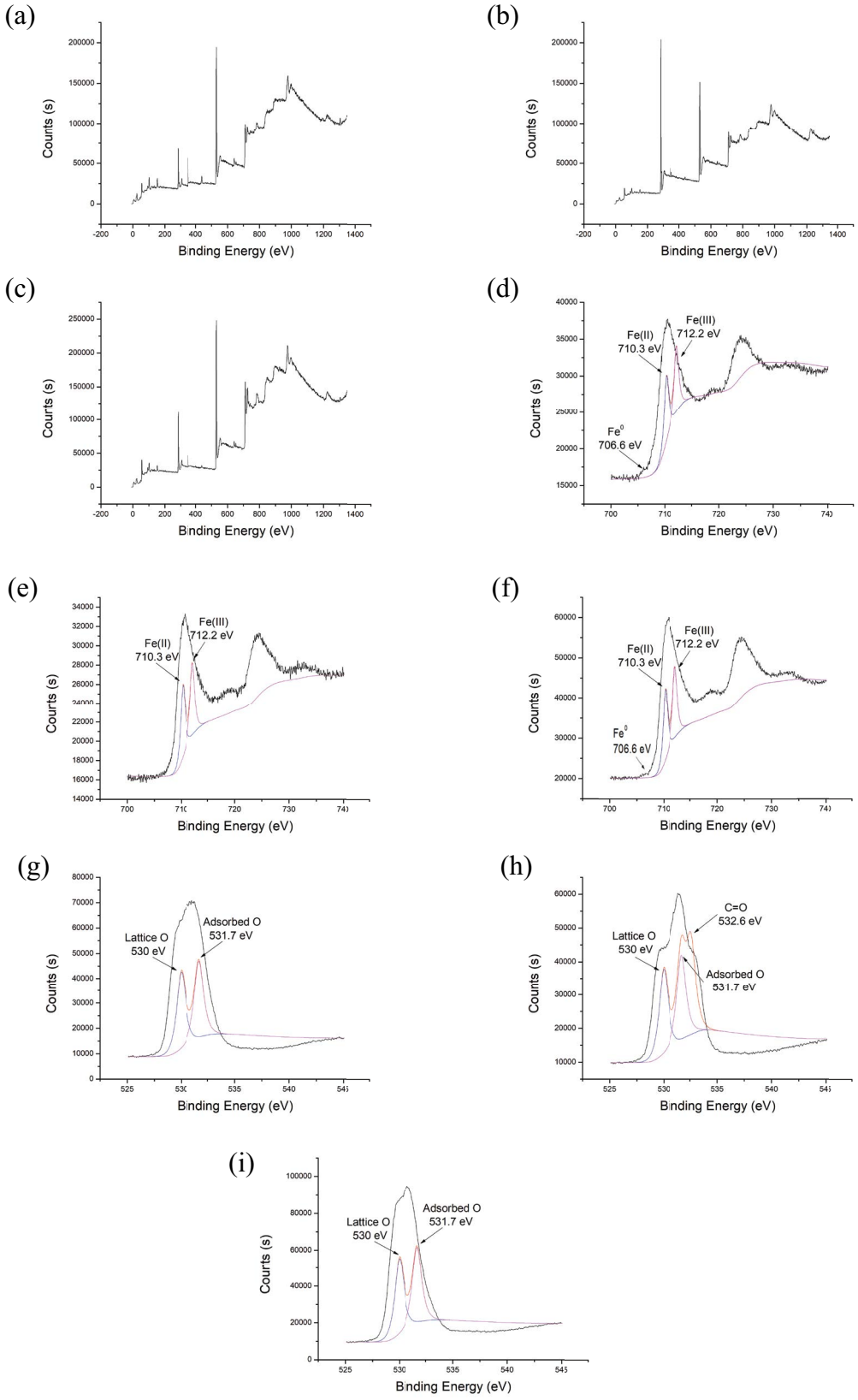

Fig. 12. XPS analysis of Fe^0 with (a) survey of original Fe^0, (b) survey of used Fe^0 without US, (c) survey of used Fe^0 with US, (d) Fe_{2p} of original Fe^0, (e) Fe_{2p} of used Fe^0 without US, (f) Fe_{2p} of used Fe^0 with US, (g) O 1s of original Fe^0, (h) O 1s of used Fe^0 without US and (i) O 1s of used Fe^0 with US.

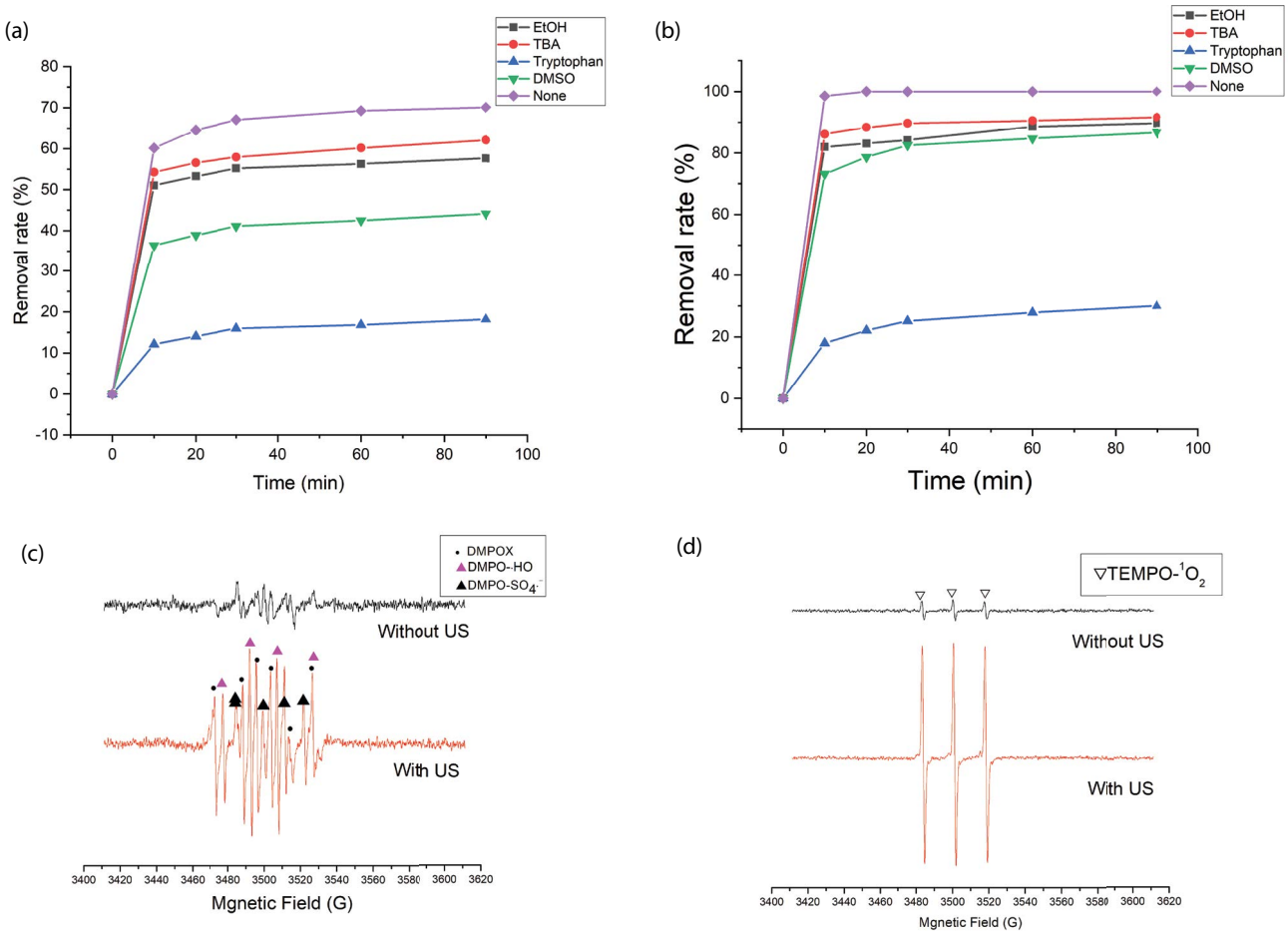

Fig. 13. Radical quenching tests (a) without US and (b) with US; Electron paramagnetic resonance tests for (c) $SO_4^{\bullet-}$, $^{\bullet}OH$, and (d) $^1O_2$.

result of the ESR and radical quenching test, $SO_4^{\bullet-}$, $^{\bullet}OH$, $^1O_2$ and Fe(IV) all played an important role in the removal of HA and $^1O_2$ was the dominant ROS for HA removal.

Acknowledgments

The authors sincerely thank the grant funded by the Study on Comprehensive Control of Rocky Desertification and Ecological Service Function Improvement in Karst Peaks (No. 2016YFC0502402). This work also was financially supported by the National Natural Science Foundation of China (No. 51709254) and the Youth Innovation Promotion Association, Chinese Academy of Sciences (No. 2020335).

References

[1] M. Sgroi, T. Anumol, F.G.A. Vagliasindi, S.A. Snyder, P. Roccaro, Comparison of the new Cl_2/O_3/UV process with different ozone- and UV-based AOPs for wastewater treatment at pilot scale: removal of pharmaceuticals and changes in fluorescing organic matter, Sci. Total Environ., 765 (2020) 142720, doi: 10.1016/j.scitotenv.2020.142720.

[2] C. Gundacker, I. Ellinger, The unique applicability of the human placenta to the Adverse Outcome Pathway (AOP) concept: the placenta provides fundamental insights into human organ functions at multiple levels of biological organization, Reprod. Toxicol., 96 (2020) 273–281.

[3] Y. Hao, H. Ma, Q. Wang, L. Ge, Y. Yang, C. Zhu, Refractory DOM in industrial wastewater: formation and selective oxidation of AOPs, Chem. Eng. J., 406 (2021) 126857, doi: 10.1016/j.cej.2020.126857.

[4] M.M. M'Arimi, C.A. Mecha, A.K. Kiprop, R. Ramkat, Recent trends in applications of advanced oxidation processes (AOPs) in bioenergy production: review, Renewable Sustainable Energy Rev., 121 (2020) 109669, doi: 10.1016/j.rser.2019.109669.

[5] C. Agarkoti, P.R. Gogate, A.B. Pandit, Comparison of acoustic and hydrodynamic cavitation based hybrid AOPs for COD reduction of commercial effluent from CETP, J. Environ. Manage., 281 (2021) 111792, doi: 10.1016/j.jenvman.2020.111792.

[6] T. Zhang, Y. Liu, S. Zhong, L. Zhang, AOPs-based remediation of petroleum hydrocarbons-contaminated soils: efficiency, influencing factors and environmental impacts, Chemosphere, 246 (2020) 125726, doi: 10.1016/j.chemosphere.2019.125726.

[7] X. Yu, J. Sun, G. Li, Y. Huang, Y. Li, D. Xia, F. Jiang, Integration of $^{\bullet}SO_4^{-}$-based AOP mediated by reusable iron particles and a sulfidogenic process to degrade and detoxify Orange II, Water Res., 174 (2020) 115622, doi: 10.1016/j.watres.2020.115622.

[8] G. Wang, Y. Zhao, H. Ma, C. Zhang, X. Dong, X. Zhang, Enhanced peroxymonosulfate activation on dual active sites of N vacancy modified g-C_3N_4 under visible-light assistance and its selective removal of organic pollutants, Sci. Total Environ., 756 (2021) 144139, doi: 10.1016/j.scitotenv.2020.144139.

[9] L. Kong, G. Fang, X. Xi, Y. Wen, Y. Chen, M. Xie, F. Zhu, D. Zhou, J. Zhan, A novel peroxymonosulfate activation process by periclase for efficient singlet oxygen-mediated

degradation of organic pollutants, Chem. Eng. J., 403 (2021) 126445, doi: 10.1016/j.cej.2020.126445.
[10] J. Zhao, F. Li, H. Wei, H. Ai, L. Gu, J. Chen, L. Zhang, M. Chi, J. Zhai, Superior performance of $ZnCoO_x$/peroxymonosulfate system for organic pollutants removal by enhancing singlet oxygen generation: the effect of oxygen vacancies, Chem. Eng. J., 409 (2021) 128150, doi: 10.1016/j.cej.2020.128150.
[11] G. Peng, C. Qi, X. Wang, L. Zhou, Q. He, W. Zhou, L. Chen, Activation of peroxymonosulfate by calcined electroplating sludge for ofloxacin degradation, Chemosphere, 266 (2021) 128944, doi: 10.1016/j.chemosphere.2020.128944.
[12] J. Yan, J. Li, J. Peng, H. Zhang, Y. Zhang, B. Lai, Efficient degradation of sulfamethoxazole by the $CuO@Al_2O_3$ (EPC) coupled PMS system: optimization, degradation pathways and toxicity evaluation, Chem. Eng. J., 359 (2019) 1097–1110.
[13] T.K. Truong, T.Q. Nguyen, H.P. Phuong La, H.V. Le, T. Van Man, T.M. Cao, V. Van Pham, Insight into the degradation of p-nitrophenol by visible-light-induced activation of peroxymonosulfate over Ag/ZnO heterojunction, Chemosphere, 268 (2021) 129291, doi: 10.1016/j.chemosphere.2020.129291.
[14] X. Ao, W. Liu, W. Sun, C. Yang, Z. Lu, C. Li, Mechanisms and toxicity evaluation of the degradation of sulfamethoxazole by MPUV/PMS process, Chemosphere, 212 (2018) 365–375.
[15] Y. Lee, S. Lee, M. Cui, Y. Ren, B. Park, J. Ma, Z. Han, J. Khim, Activation of peroxodisulfate and peroxymonosulfate by ultrasound with different frequencies: impact on ibuprofen removal efficient, cost estimation and energy analysis, Chem. Eng. J., 413 (2020) 127487, doi: 10.1016/j.cej.2020.127487.
[16] X. Li, Z. Liu, Y. Zhu, L. Song, Z. Dong, S. Niu, C. Lyu, Facile synthesis and synergistic mechanism of $CoFe_2O_4$@three-dimensional graphene aerogels towards peroxymonosulfate activation for highly efficient degradation of recalcitrant organic pollutants, Sci. Total Environ., 749 (2020) 141466, doi: 10.1016/j.scitotenv.2020.141466.
[17] R. Wang, X. Zhang, L. Zhao, J. Feng, T. Wei, Y. Ren, Y. Shen, In-situ synthesis of Fe and O co-doped g-C_3N_4 to enhance peroxymonosulfate activation with favorable charge transfer for efficient contaminant decomposition, J. Taiwan Inst. Chem. Eng., 115 (2020) 198–207.
[18] H. Dai, W. Zhou, W. Wang, Co/N co-doped carbonaceous polyhedron as efficient peroxymonosulfate activator for degradation of organic pollutants: role of cobalt, Chem. Eng. J., 417 (2020) 127921, doi: 10.1016/j.cej.2020.127921.
[19] X. Zhou, H. Luo, B. Sheng, X. Chen, Y. Wang, Q. Chen, J. Zhou, Cu^{2+}/Cu^{+} cycle promoted PMS decomposition with the assistance of Mo for the degradation of organic pollutant, J. Hazard. Mater., 411 (2021) 125050, doi: 10.1016/j.jhazmat.2021.125050.
[20] M. Kohantorabi, G. Moussavi, S. Giannakis, A review of the innovations in metal- and carbon-based catalysts explored for heterogeneous peroxymonosulfate (PMS) activation, with focus on radical vs. non-radical degradation pathways of organic contaminants, Chem. Eng. J., 411 (2020) 127957, doi: 10.1016/j.cej.2020.127957.
[21] J. Deng, M. Xu, Y. Chen, J. Li, C. Qiu, X. Li, S. Zhou, Highly-efficient removal of norfloxacin with nanoscale zero-valent copper activated persulfate at mild temperature, Chem. Eng. J., 366 (2019) 491–503.
[22] S. Chen, J. Deng, C. Ye, C. Xu, L. Huai, X. Ling, J. Li, X. Li, Degradation of p-arsanilic acid by pre-magnetized Fe^0/persulfate system: kinetics, mechanism, degradation pathways and DBPs formation during subsequent chlorination, Chem. Eng. J., 410 (2021) 128435, doi: 10.1016/j.cej.2021.128435.
[23] S. Chen, J. Deng, C. Ye, C. Xu, L. Huai, J. Li, X. Li, Simultaneous removal of para-arsanilic acid and the released inorganic arsenic species by $CuFe_2O_4$ activated peroxymonosulfate process, Sci. Total Environ., 742 (2020) 140587, doi: 10.1016/j.scitotenv.2020.140587.
[24] W. Chen, Z. Gu, S. Guo, Q. Li, Microwave-assisted Fe^0-activated persulfate process for treating explosives in production wastewater, Chem. Eng. J., 391 (2020) 123497, doi: 10.1016/j.cej.2019.123497.
[25] K. Zhu, H. Xu, C. Chen, X. Ren, A. Alsaedi, T. Hayat, Encapsulation of Fe^0-dominated Fe_3O_4/Fe^0/Fe_3C nanoparticles into carbonized polydopamine nanospheres for catalytic degradation of tetracycline via persulfate activation, Chem. Eng. J., 372 (2019) 304–311.
[26] Y. Pan, M. Zhou, J. Cai, X. Li, W. Wang, B. Li, X. Sheng, Z. Tang, Significant enhancement in treatment of salty wastewater by pre-magnetization Fe^0/H_2O_2 process, Chem. Eng. J., 339 (2018) 411–423.
[27] S. Yang, P. Wu, Q. Ye, W. Li, M. Chen, N. Zhu, Efficient catalytic degradation of bisphenol A by novel Fe^0-vermiculite composite in photo-Fenton system: mechanism and effect of iron oxide shell, Chemosphere, 208 (2018) 335–342.
[28] A.F. Duprat, P. Capdevielle, M. Maumy, Aromatic O-demethylation with the [Fe^0/acetic acid/O_2] system, J. Mol. Catal., 77 (1992) L7–L11.
[29] W. Liu, J. Lian, J. Guo, Y. Guo, L. Yue, Y. Niu, L. Duan, Perchlorate bioreduction by anaerobic granular sludge immobilised with Fe-HA complex: performance, extracellular polymeric substances and microbial community structure, J. Hazard. Mater., 398 (2020) 122898, doi: 10.1016/j.jhazmat.2020.122898.
[30] X. Li, B. Wu, Q. Zhang, Y. Liu, J. Wang, F. Li, F. Ma, Q. Gu, Complexation of humic acid with Fe ions upon persulfate/ferrous oxidation: further insight from spectral analysis, J. Hazard. Mater., 399 (2020) 123071, doi: 10.1016/j.jhazmat.2020.123071.
[31] J. Yao, Y. Yu, R. Qu, J. Chen, Z. Huo, F. Zhu, Z. Wang, Fe-activated peroxymonosulfate enhances the degradation of dibutyl phthalate on ground quartz sand, Environ. Sci. Technol., 54 (2020) 9052–9061.
[32] J. Hu, H. Chen, H. Dong, L. Zhu, Z. Qiang, J. Yu, Transformation of iopamidol and atrazine by peroxymonosulfate under catalysis of a composite iron corrosion product (Fe/Fe_3O_4): electron transfer, active species and reaction pathways, J. Hazard. Mater., 403 (2021) 123553, doi: 10.1016/j.jhazmat.2020.123553.
[33] Y. Tang, J. Kang, M. Wang, C. Jin, J. Liu, M. Li, S. Li, Z. Li, Catalytic degradation of oxytetracycline via $FeVO_4$ nanorods activating PMS and the insights into the performance and mechanism, J. Environ. Chem. Eng., 9 (2021) 105864, doi: 10.1016/j.jece.2021.105864.
[34] J. Peng, Z. Wang, S. Wang, J. Liu, Y. Zhang, B. Wang, Z. Gong, M. Wang, H. Dong, J. Shi, H. Liu, G. Yan, G. Liu, S. Gao, Z. Cao, Enhanced removal of methylparaben mediated by cobalt/carbon nanotubes (Co/CNTs) activated peroxymonosulfate in chloride-containing water: reaction kinetics, mechanisms and pathways, Chem. Eng. J., 409 (2021) 128176, doi: 10.1016/j.cej.2020.128176.
[35] X. Li, X. Liu, C. Lin, Z. Zhou, M. He, W. Ouyang, Catalytic oxidation of contaminants by Fe^0 activated peroxymonosulfate process: Fe(IV) involvement, degradation intermediates and toxicity evaluation, Chem. Eng. J., 382 (2020) 123013, doi: 10.1016/j.cej.2019.123013.
[36] T. Huang, G. Zhang, N. Zhang, J. Ye, P. Lu, Fe^0-H_2O_2 for advanced treatment of citric acid wastewater: detailed study of catalyst after several times use, Chem. Eng. J., 336 (2018) 233–240.
[37] Y. Yan, H. Zhang, W. Wang, W. Li, Y. Ren, X. Li, Synthesis of Fe^0/Fe_3O_4@porous carbon through a facile heat treatment of iron-containing candle soots for peroxymonosulfate activation and efficient degradation of sulfamethoxazole, J. Hazard. Mater., 411 (2021) 124952, doi: 10.1016/j.jhazmat.2020.124952.
[38] J. Cao, L. Lai, B. Lai, G. Yao, X. Chen, L. Song, Degradation of tetracycline by peroxymonosulfate activated with zero-valent iron: performance, intermediates, toxicity and mechanism, Chem. Eng. J., 364 (2019) 45–56.
[39] Z. Li, K. Li, S. Ma, B. Dang, Y. Li, H. Fu, J. Du, Q. Meng, Activation of peroxymonosulfate by iron-biochar composites: comparison of nanoscale Fe with single-atom Fe, J. Colloid Interface Sci., 582 (2021) 598–609.
[40] J. Liu, J. Zhou, Z. Ding, Z. Zhao, X. Xu, Z. Fang, Ultrasound irritation enhanced heterogeneous activation of peroxymonosulfate with Fe_3O_4 for degradation of azo dye, Ultrason. Sonochem., 34 (2017) 953–959.
[41] M. Li, R. Luo, C. Wang, M. Zhang, W. Zhang, P.K. Klu, Y. Yan, J. Qi, X. Sun, L. Wang, J. Li, Iron-tannic modified cotton derived Fe^0/graphitized carbon with enhanced catalytic activity for bisphenol A degradation, Chem. Eng. J., 372 (2019) 774–784.

[42] B. Liu, W. Song, H. Wu, Y. Xu, Y. Sun, Y. Yu, H. Zheng, S. Wan, Enhanced oxidative degradation of norfloxacin using peroxymonosulfate activated by oily sludge carbon-based nanoparticles $CoFe_2O_4$/OSC, Chem. Eng. J., 400 (2020) 125947, doi: 10.1016/j.cej.2020.125947.
[43] G. Zhao, J. Zou, X. Chen, L. Liu, Y. Wang, S. Zhou, X. Long, J. Yu, F. Jiao, Iron-based catalysts for persulfate-based advanced oxidation process: microstructure, property and tailoring, Chem. Eng. J., 421 (2020) 127845, doi: 10.1016/j.cej.2020.127845.

Supplementary information

S1. Materials and methods

S1.1. Materials and instruments

S1.1.1. Materials

Zero-price iron was purchased from Beijing Deco Island Gold Technology Co., Ltd. Humic acid (HA) was obtained from the International Humic Acid Association. Potassium peroxymonosulfate (PMS), sulfuric acid, dimethyl sulfoxide, sodium hydroxide, ethanol, tert-butanol, dimethylpyridine N-oxide, 2,2,6,6-tetramethylpiperidine-1-oxyl, methyl phenyl sulfoxide and tryptophan were provided by Sigma-Aldrich (China). All chemicals used in the experiments were analytical grade and used without further purification. Ultrapure water derived from Millipore Water Purification System was employed throughout the experiments.

S1.1.2. Instruments

X-ray diffraction (XRD) spectra were recorded by diffractometer (D8 ADVANCE). The surface element states were analyzed using an X-ray Photoelectron Spectrometer (ESCALAB XI^+). The surface topography and elemental composition of zero-valent iron (Fe^0) were observed using a scanning electron microscope (JSM-IT300) and transmission electron microscopy (Tecnai F20). Specific surface area and zeta potential were analyzed by Brunauer–Emmett–Teller (MIKE 2020) and zeta potential analyzer (ZetaPALS), respectively. Electron paramagnetic resonance (Brook A300) was used to capture the radical produced in the solution. The concentration of iron leaching was measured using an inductively coupled plasma mass spectrometer (PerkinElmer, America). An X-ray Fluorescence Spectrometer (PANalytical Axios, Netherlands) was used to analyze the excitation–emission matrix spectra (EEM) of the HA solution. The concentration of the solution was analyzed using a UV-Vis spectrophotometer (UNICOWFUV-2).

Table S1
pH change after reaction

Initial pH	pH after reaction (without US)	pH after reaction (with US)
3	3.8	4.3
5	5.7	6.1
7	7.2	7.4
9	8.5	8.2
11	10.6	9.9

Table S2
TOC removal rate under different systems

Recycle experiment	TOC removal rate without US (%)	TOC removal rate with US (%)
(First use) Fe^0	34.6	43.7
(Second use) Fe^0	26.2	40.2
(Third use) Fe^0	17.2	35.1
(Fourth use) Fe^0	7.8	28.4

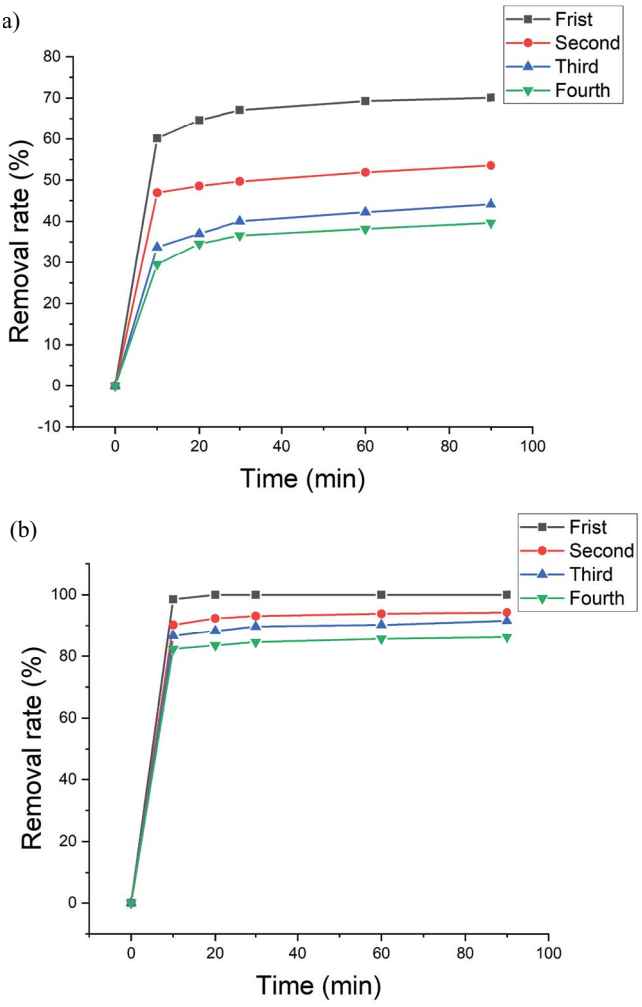

Fig. S1. Cycle utilization of Fe^0 (a) without US and (b) with US.

A shaker (SHZ-2A) and an ultrasound machine (KQ 100DE) with 100 W power were used throughout the experiment.

S1.2. Experimental work

100 mL of HA solution, PMS solution and Fe^0 were added was added into 150 mL flasks. 1 M H_2SO_4 and 1 M NaOH were employed to adjust the pH value of the solution. In the condition without ultrasound (US), the flask was set in a shaker with a speed of 200 rpm and a temperature of 25°C. In the condition of without US, the flask

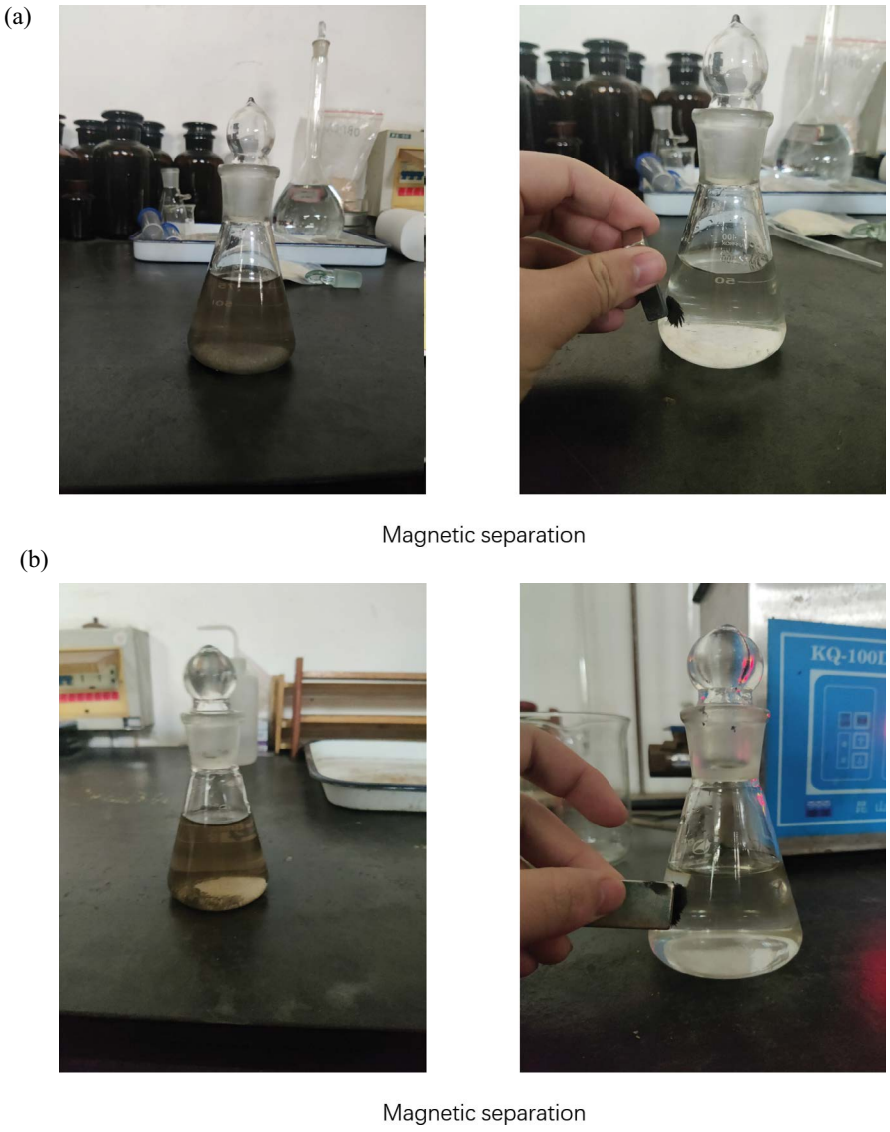

Fig. S2. The photograph of Fe^0 before reaction (left) and magnetic separation after reaction (right): (a) without US and (b) with US.

was set in an ultrasound tank with 100 W power. At certain time intervals, 5 mL of the solution in the flask was collected and filtered with a syringe filter. In the cycling experiment of Fe^0, Fe^0 was collected using magnetic separation. The concentration of HA was determined using a UV spectrometer at 254 nm. The removal rate of humic acid is calculated according to Eq. (S1):

$$\text{Removal rate} = \frac{C_0 - C_t}{C_0} \quad \text{(S1)}$$

where C_0 is the initial HA concentrations; C_t is the concentration of HA at time t.

S1.3. Quenching tests for reactive oxygen species

Four quenching agents, including ethanol, tert-butanol, methyl phenyl sulfoxide and tryptophan, were employed as a scavenger for the reactive oxygen species. Ethanol

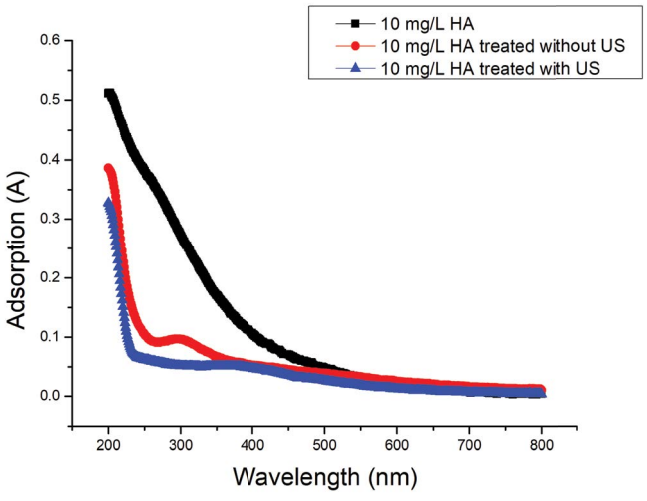

Fig. S3. UV-Vis of 10 mg/L HA solution.

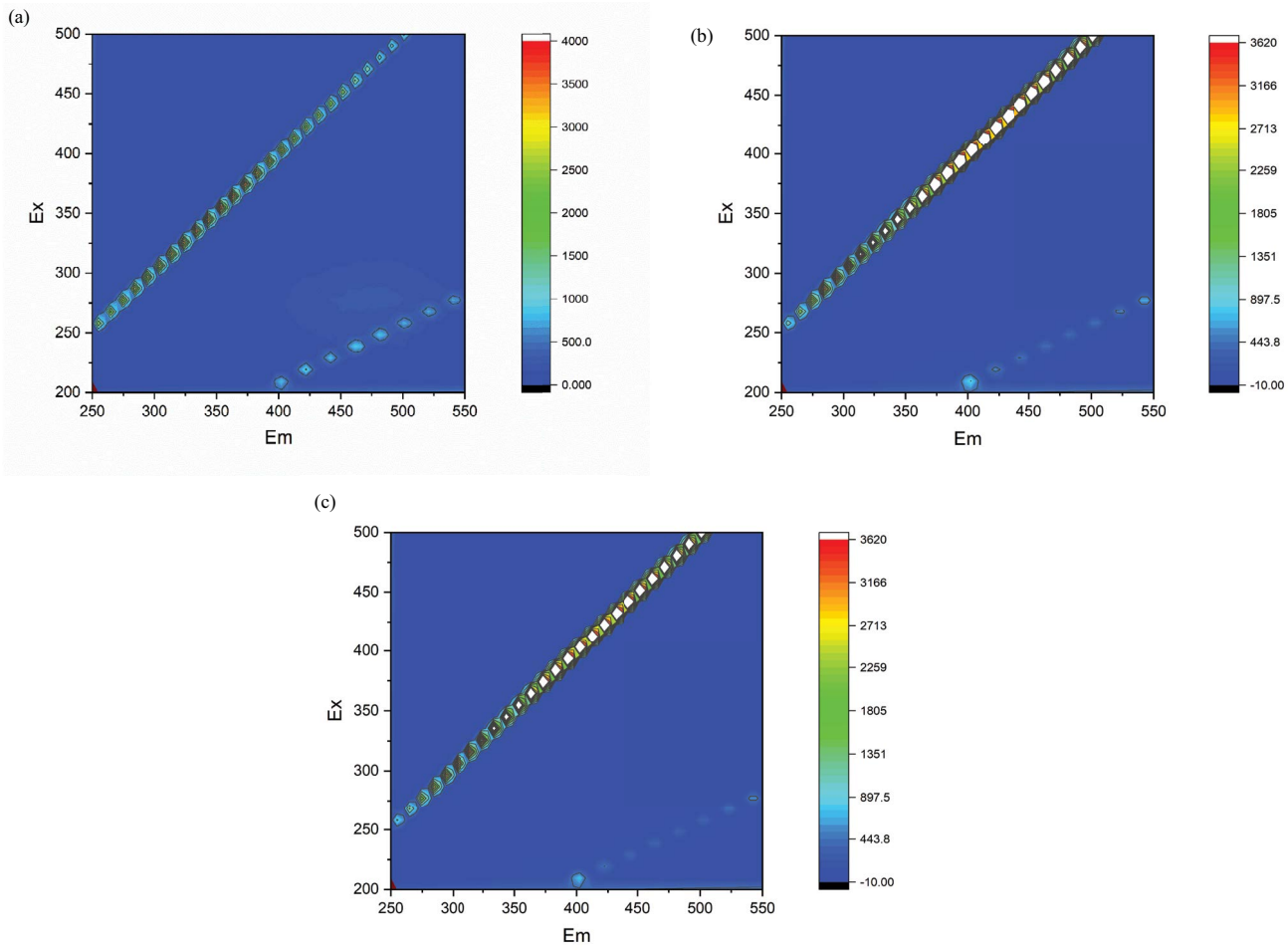

Fig. S4. EEM of 10 mg/L HA solution: (a) untreated HA solution, (b) treated HA solution by Fe^0/PMS system and (c) treated HA solution by Fe^0/PMS/US.

was used to scavenge $SO_4^{\bullet-}$ and $^{\bullet}OH$. Tert-butanol and tryptophan were used to scavenger $^{\bullet}OH$ and $^1O_2$, respectively. Methyl phenyl sulfoxide was used to quench Fe(IV). The molar concentration ratios of PMS and quenching agents were fitted as 1 to 100.

S1.4. Thermal effect and non-thermal effect of US

To study the thermal effects form US radiation for HA removal, the temperature in US tank was set at 40°C (close to the reaction temperature) and 25°C (using a self-made circulating water cooling system). As the control experiment, the temperature set at 40°C and 25°C without US was also carried out.